Chemical Science

ROYAL SOCIETY OF CHEMISTRY

EDGE ARTICLE

View Article Online
View Journal | View Issue

Cite this: *Chem. Sci.*, 2025, **16**, 13022

All publication charges for this article have been paid for by the Royal Society of Chemistry

Single-molecule contact switching *via* electro-inductive effects†

Ya-Li Zhang,‡ Tian-Hang Bai,‡ Jing-Tao Ye,‡ Li-Na Luo, Qiang Wan, * Ju-Fang Zheng, Yong Shao, Ya-Hao Wang * and Xiao-Shun Zhou *

Received 24th March 2025
Accepted 6th June 2025

DOI: 10.1039/d5sc02252e

rsc.li/chemical-science

The non-faradaic application of electric fields generated at the surface of charged electrodes to polarize bound molecules, also termed as electro-inductive effects, have recently attracted increasing attention in modifying the chemical reactivity of molecules in electrosynthesis. Herein, we applied this electro-inductive effect to control the Lewis adduct formation and dissociation between BF_3 and pyridine N of heterocycles to realize single-molecule contact switching. *In situ* single-molecule conductance measurements, *in situ* Raman analysis and theoretical calculations clearly show that the outward electric field along the positively-charged electrode surface polarizes adsorbed molecules to withdraw electron density from the terminal pyridine N, which weakens the N–BF_3 Lewis bond for dissociation upon applied positive potentials. The released unbounded pyridine N can connect the molecule into a molecular circuit for electron transfer (considered as the "ON" state). Meanwhile, the inward electric field along the negatively charged electrode surface promotes the formation of an N–BF_3 Lewis bond, leading to breaking of the molecular circuit (considered as the "OFF" state). Combined with the optimization of BF_3 concentration from the equilibrium $BF_4^- \rightleftharpoons BF_3 + F^-$, the electro-inductive effect can reversibly switch single-molecule conductance in conductance measurements and tunnelling currents in *I*–*V* measurements.

Introduction

Since the first prototype of a single-molecule rectifier proposed by Aviram and Ratner in 1974,[1] many studies have used various anchoring groups as "alligator clips" to connect single molecules into two metal electrode nanogaps,[2–4] which provide an ideal test platform for exploring electron transport at the single-molecule scale.[5–7] Using these chemical linkers like thiols,[8,9] thioethers,[10,11] amines[8,12] and pyridines,[8,13–16] much effort has been devoted to the design of stimuli-responsive functional molecules, and they have been integrated into electric circuits to show the possibility and capability of single-molecule devices.[17–22] However, the nature of molecule-metal contacts greatly determines the electron conduction and the current–voltage characteristics *via* modification of the molecular adsorption geometry and interfacial coupling between the discrete molecular orbitals and the electronic bands of the electrodes.[23–26] For example, recent experiments have demonstrated that tuning interfacial molecule-metal contacts *via* electrical and mechanical means can achieve the functionality of a molecular switch.[27–29] However, using external control to reversibly disconnect or connect molecule-metal contacts remains a challenge, and single-molecule circuits can be physically turned on and off, promising molecular switches with large ON/OFF ratios.[30–32]

Electric fields have been shown to play a key role in many types of catalytic chemical reactions.[33,34] Very recently, the interfacial electric field near an electrode induced by an applied potential[35,36] has been shown to be analogous to the effect of electron withdrawing/donating substituents, which could continuously modulate the electronic properties of surface-bound molecules to change their chemical reactivity in electrosynthesis. This non-faradaic use of polarized electrochemical interfaces, termed as the electro-inductive effect in 2020, has attracted increasing attention.[35] For example, the electro-inductive effect has been shown to activate aromatic molecules toward redox neutral hydrolysis, crosscoupling, and amidation reactions, and control formation and dissociation of N-heterocycle-BF_3 Lewis adducts.[35,37,38] This electrochemical polarization may provide a new, yet unexplored, approach to control interfacial molecule-metal contacts in molecular junctions to achieve switching functionality.

In this work, we first used a scanning tunnelling microscope-based break junction (STM-BJ) method[4,39–41] to reveal the electro-inductive effect on molecule-metal contacts in single-

Key Laboratory of the Ministry of Education for Advanced Catalysis Materials, Institute of Physical Chemistry, College of Chemistry and Materials Science, Zhejiang Normal University, Jinhua 321004, P. R. China. E-mail: xszhou@zjnu.edu.cn; yahaowang@zjnu.edu.cn; qiangwan@zjnu.edu.cn

† Electronic supplementary information (ESI) available. See DOI: https://doi.org/10.1039/d5sc02252e

‡ Ya-Li Zhang, Tian-Hang Bai, Jing-Tao Ye, contributed equally to this work.

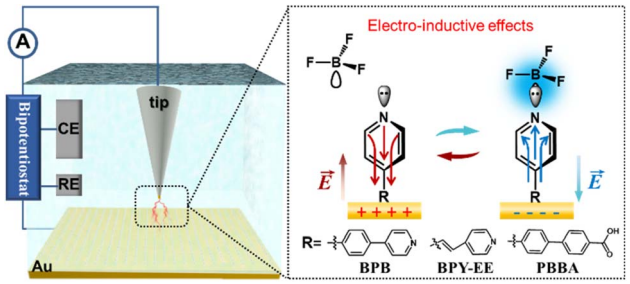

Scheme 1 Schematic diagram of STM-BJ methods used to probe the electro-induced effect of the N–BF_3 Lewis bond in $LiBF_4$ solution, which can regulate metal-molecule contacts in the single-molecule junction for switching.

molecule junctions. As schematically illustrated in Scheme 1, at a positively charged surface, the outward electric field along the electrode surface polarizes the adsorbed molecules to withdraw electron density from the pyridine nitrogen (denoted as N). This can weaken the Lewis bond of N–BF_3 and even make it dissociate. The released pyridine group can interact with the STM tip to form a molecular junction to allow electron transport (ON state). Conversely, at a negatively charged surface, the inward electric field pushes electron density toward the N, which promotes the formation of N-heterocycle-BF_3 Lewis adducts. This causes the molecules to be unable to connect with the STM tip, thereby achieving a circuit break (OFF state).

A propylene carbonate (PC) solution containing $LiBF_4$ is used because BF_3 can be liberated from $LiBF_4$ based on the equilibrium $BF_4^- \rightleftharpoons BF_3 + F^-$ in this system according to previous reports.[37] In this way, the electrochemical control of $BF_3 + N \rightleftharpoons$ N–BF_3 *via* electro-inductive effects can be used to reversibly tune the metal-molecule contacts in the molecular junctions. Electrochemical STM-BJ clearly shows the conductance peaks as a result of the formation of the single-molecule junction, dependent on the applied potential as well as the types and concentrations of electrolytes. *In situ* Raman spectroscopic evidence and theoretical calculations also confirm that the reversible single-molecule conductance switching can be ascribed to electro-inductive effects on this N-heterocycle–BF_3 Lewis adduct. Furthermore, *I–V* measurements performed in a fixed nanogap between the STM tip and substrate confirmed the feasibility of physically disconnecting or connecting single-molecule circuits, providing a new approach to achieve a reversible single-molecule switch *via* electro-inductive effects.

Results and discussion

The influence of Lewis bonds on single-molecule conductance

We first selected 1,4-bis(pyridin-4-yl)benzene (BPB) with pyridine groups as a target molecule, which has a very well-defined single molecule conductance peak in previous reports.[42,43] To obtain the intrinsic conductance information of molecular junctions, conductance measurements (see experimental details in ESI†) by using STM-BJ were carried out in a PC solution of 0.1 mM BPB, 0.1 mM BPB + 50 mM $LiBF_4$ or 0.1 mM BPB + 50 mM $LiNO_3$. As shown in Fig. 1a, the representative conductance-displacement traces show step features at about $10^{-3.8}$ G_0 ($G_0 = 2e^2/h$, where e is the electron charge and h is Planck's constant) both in 0.1 mM BPB and 0.1 mM BPB + 50 mM $LiNO_3$ solution. Meanwhile, there are only decay traces observed in 0.1 mM BPB + 50 mM $LiBF_4$ solution. Typically, these step features are ascribed to the formation of single-molecule junctions after rupturing Au atomic contacts during the stretching process of the tip. This indicates that the formation of BPB molecular junctions could be obstructed in the solution containing 50 mM $LiBF_4$. 1000 individual conductance-displacement traces are used to construct 1D conductance histograms in Fig. 1b, showing a well-defined conductance peak at $10^{-3.8}$ G_0 in solution without $LiBF_4$, in contrast to only a blank background in $LiBF_4$ solution. This reveals that the BF_3 from BF_4^- dissociation forms a Lewis bond with the pyridine N in the molecule, and the N–BF_3 cannot bind to the Au electrodes to form a molecular junction.

We also statistically analyze stretching displacements (z) in each conductance-displacement trace from $10^{-6.0}$ to $10^{-0.3}$ G_0, consistent with previous reports.[40,44,45] The two-dimensional (2D) conductance histogram in Fig. 1c clearly shows an obvious stretching state centered around $10^{-3.8}$ G_0 after rupturing Au atomic contacts, and the Δz of 0.6 nm is found by Gaussian fitting. By adding the snapback distance (0.5 nm) of breaking Au atomic contacts, the most probable absolute displacement for molecular junctions is about 1.1 nm, comparable to the BPB molecular length of 1.15 nm. This proves the formation of single-molecule junctions.

To further clarify the Lewis bond effect on the formation of molecular junctions, single-molecule conductance measurements were also carried out in 0.1 mM BPB solution with different concentrations of $LiBF_4$. It can be expected that the equilibrium $BF_4^- \rightleftharpoons BF_3 + F^-$ shifts in the opposite direction when decreasing the concentration of BF_4^-, resulting in less BF_3 in solution to interact with BPB molecules. The conductance histograms in Fig. 1d clearly show that the conductance peak appears at 30 mM $LiBF_4$, and becomes more intense as the concentration of $LiBF_4$ is further decreased. Finally, the conductance peak at 10 mM $LiBF_4$ is comparable with that in a pure molecule solution. Controlled experiments using the target molecule 1,4-bis((2,3-dihydrobenzo[*b*]thiophen-5-yl) ethynyl) benzene without pyridine groups do not show such a conductance peak transition (Fig. S1†). This strongly supports the idea that the molecules almost turn into an N–BF_3 Lewis adduct when the concentration of $LiBF_4$ is greater than 40 mM. Then, the N–BF_3 cannot bind to the Au electrode to form molecular junctions.

The UV-vis spectra in Fig. 1e also reveal that the absorption peak of the 0.1 mM BPB solution red shifts when changing the concentration of $LiBF_4$ from 10 mM to 50 mM. The absorption peaks can be Gaussian fitted into two peaks centred at 280 nm and 312 nm, corresponding to BPB and BPB-BF_3 species, respectively (Fig. S2†). An obvious peak transition state can be observed at 20 mM. Such an absorption peak transition state can be observed for these diluted samples (Fig. S3†). This suggests that the formation of an N–BF_3 Lewis bond can be completed in bulk PC solution. Previous reports[37,38] found that

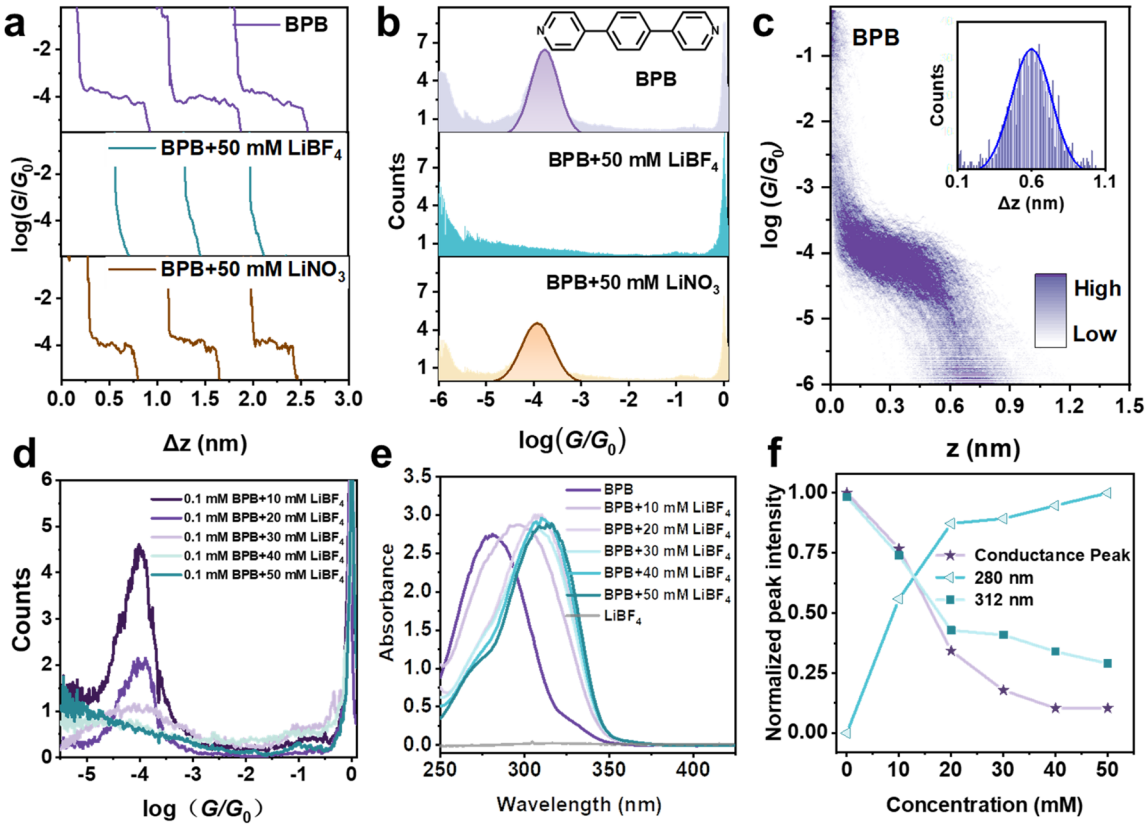

Fig. 1 (a) Representative conductance-displacement traces and (b) 1D conductance histograms obtained in PC solution of 0.1 mM BPB (purple), 0.1 mM BPB + 50 mM $LiBF_4$ (blue) and 0.1 mM BPB + 50 mM $LiNO_3$ (yellow). (c) 2D conductance-displacement histograms of BPB molecular junctions. The inset panel shows the corresponding relative stretching distance distribution. (d) 1D conductance histograms of BPB molecular junctions obtained in $LiBF_4$ solutions with different concentrations. (e) UV-vis absorption spectra of 0.1 mM BPB solution with different concentrations of $LiBF_4$. (f) Plot of normalized Gaussian-fitted conductance peak intensity and UV-vis absorption peak intensity as a function of electrolyte concentration.

when one pyridine group forms a Lewis bond with BF_3, the UV-vis absorption peak undergoes a 70 nm red shift. In addition, theoretical simulations in Fig. S4† show that when the single-terminal pyridine group of the BPB molecule is combined with BF_3, its absorption peak is red-shifted by 20 nm, consistent with experimental results. Fig. 1f compares the Gaussian-fitted conductance peak intensity and UV-vis absorption peak intensity as a function of electrolyte concentration. This nonlinear correlation between conductance peak intensity and molecular concentration in solution is consistent with previous reports.[46,47] Notably, the most significant conductance peak intensity reduction occurs at 20 mM $LiBF_4$ when most of the BPB molecules turn into BPB-BF_3 in the solution, indicated by the absorption peak variation. This proves that the N–BF_3 Lewis bond at one terminal pyridine group of the molecule suppresses the molecular junction formation.

Electro-inductive effects of the Lewis bond in single-molecule junctions

To investigate the electro-inductive effects of the Lewis bond in single-molecule junctions, the four-electrode setup of electrochemical STM is used to perform conductance measurements in 0.1 mM BPB + 30 mM $LiBF_4$ solution. In this configuration, the potentials of the Au (111) substrate ($E_{substrate}$) could be adjusted relative to the reference electrode. Cyclic voltammograms (CVs) of BPB on an Au electrode in Fig. S5† do not show any redox peak in the potential window of −0.8 V to 0.2 V. In line with the CV profile, conductance measurements were carried out in the same potential range with a 0.2 V interval. As shown in Fig. 2a, there is no conductance peak observed until the applied potentials of the Au(111) substrate ($E_{substrate}$) increase to −0.2 V and above. The measurements of the potential of zero charge (PZC) in Fig. S6† exhibited a −0.22 V value for Au (111) in 0.1 mM BPB + 30 mM $LiBF_4$ solution. This reveals that the Au electrode surface is positively charged above −0.22 V. It generates an electric field outward along the electrode surface to withdraw the electron density from the terminal N of adsorbed molecules and makes the N–BF_3 Lewis bond dissociate. Thus, the unbonded N can bind to the Au tip to form a molecular junction, resulting in the appearance of a conductance peak. Fig. S7† also shows that the distinct conductance peaks attributed to BPB molecular junctions were consistently observed in $LiNO_3$ solution, indicating that the interfacial electric fields generated under applied potentials cannot completely suppress pyridine–Au interaction.

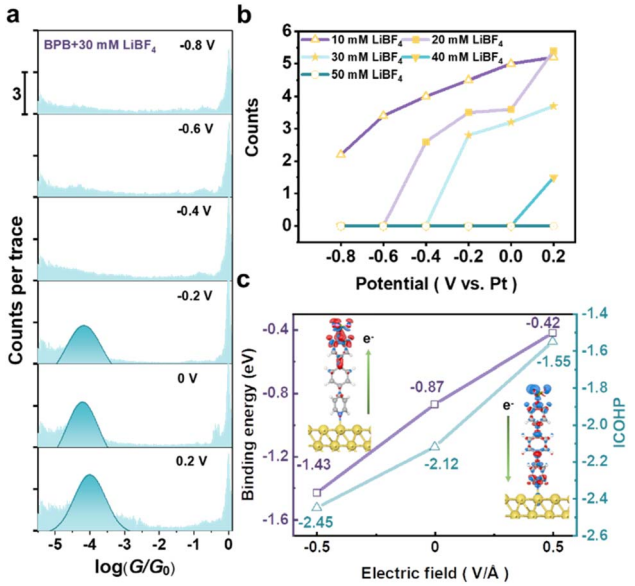

Fig. 2 (a) 1D conductance histograms obtained at different applied $E_{substrate}$ values in 0.1 mM BPB + 30 mM $LiBF_4$. (b) Plot of the conductance peak intensities of BPB molecular junctions against the applied $E_{substrate}$ in $LiBF_4$ solution with different concentrations. (c) Binding energies of BF_3 on N and ICOHP values for the N–BF_3 Lewis bond under different electric fields. A more negative ICOHP indicates a lower energy bonding state and higher bond strength. The inset panels show electron density difference ($\Delta\rho = \rho_{(+0.5/-0.5)} - \rho_0$) diagrams for BPB adsorption on Au(111), where $\rho_{(+0.5/-0.5)}$ and ρ_0 are the electron density with and without the electric field, respectively. The red region represents the accumulation of electrons while the blue one represents depletion. Isovalue = 0.005 e Å^{-3}.

Furthermore, we also changed the $LiBF_4$ concentration in the solutions to investigate the electro-inductive effects of the N–BF_3 Lewis bond. Detailed conductance histograms at different $E_{substrate}$ values can be found in Fig. S8.† Fig. 2b summarizes the conductance peak intensities of BPB molecular junctions against the applied $E_{substrate}$ in $LiBF_4$ solution with different concentrations. In 10 mM $LiBF_4$ solution, the conductance peak exists in the electrochemical window from 0.2 V to −0.8 V, but its intensity weakens as the potential decreases. This means that when the BF_3 concentration in the solution is low, the inductive effect at negative potentials cannot convert adsorbed molecules into enough Lewis adducts, thereby reducing the probability of forming a molecular junction to a low enough level that no conductance peak can be observed.

Interestingly, in the $LiBF_4$ solution with concentration ranges of 20–40 mM, as the potential decreases from 0.2 V, the conductance peak intensity decreases, and the potential at which it disappears is significantly advanced as the concentration increases. When the electrolyte concentration reaches 50 mM, no conductance peak can be detected in the entire electrochemical window. This suggests that when the electrode surface carries more negative charges, a stronger electron-donating inductive effect will occur, promoting the formation of N–BF_3 Lewis bonds. However, the BF_3 concentration in solution is also crucial to achieve the complete suppression of the molecular junction formation. The formation of a single-molecule junction requires only a certain surface coverage of the unbonded molecules, in line with the previous reports.[43,46,48] Utilizing the electro-inductive effects can also regulate the interaction between Lewis basic pyridyl N and Lewis acid $Al(CH_3)_3$, which enables controllable modulation of single-molecule contacts in molecular junctions (Fig. S9†).

To gain a greater understanding of the electro-inductive effects on the N–BF_3 Lewis bonds, we further compared their behaviour under opposite electric field directions. The electric field strength was set to 0.5 V Å^{-1}.[49,50] The results show that the N–BF_3 bond (Fig. S10†) elongates and the binding energy (Fig. 2c) of BF_3 on N becomes less negative (−1.43 to −0.42 eV) as the electric field switches from −0.5 to 0.5 V Å^{-1}, suggesting that the Lewis acid–base interaction between BF_3 and N is suppressed by an outward electric field (positively charged surface). Further analyses of the electronic structures of N–BF_3 bonds were conducted by utilizing crystal orbital Hamiltonian population (COHP). As shown in Fig. S11,† a shift in the occupied bonding states towards the Fermi level was observed when the field was switched from −0.5 to 0.5 V Å^{-1}. This suggests an increase in bonding state energy, leading to reduced N–BF_3 stability.

Quantitatively, under an inward electric field (negatively charged surface), the integrated COHP (ICOHP) value becomes more negative (Fig. 2c) which indicates a stronger N–BF_3 bond. This trend can be attributed to the distinctly different electron transfer under various electric fields. Specifically, the direction of electron transfer under the two opposite electric fields aligned with the charge transfer direction of the bare Au(111) surface (Fig. S12†). As shown in the inset panels of Fig. 2c, under an inward electric field, electrons transfer from the surface to the BF_3 termination (in line with the N–B dipole), while under an outward electric field, electrons are transferred from the BF_3 termination to the Au surface (opposite to the N–B dipole). The distinctly different electron transfer results in a strengthening and weakening of the polar B–N bond, respectively. The adsorption strength of BPB-BF_3 on Au(111) is much weaker than that of BPB (Fig. S13†), suggesting its difficulty to form molecular junctions.

Interfacial molecular evidence

To investigate and elaborate the interfacial molecular structures upon different electro-inductive effects, we performed *in situ* Raman analysis by using shell-isolated nanoparticle enhanced Raman spectroscopy[51–53] (SHINERS, See the experimental details in the ESI†). This typically used Au core–SiO_2 shell nanoparticles as Raman-signal amplifiers (Fig. S14†) and could effectively work on a single-crystal surface. Fig. 3a shows the potential-dependent Raman spectra in 0.1 mM BPB + 30 mM $LiBF_4$ solution from 0.2 V to −0.8 V with 0.1 V intervals. It is clear that the intense Raman bands at 1031, 1225, 1291, and 1609 cm^{-1} can be ascribed to the pyridyl ring breathing mode, in-plane CH bending, inter-ring stretching and parallel CC stretching of the BPB molecule, consistent with previous reports.[51,54] The Raman signals of the BPB molecule can be

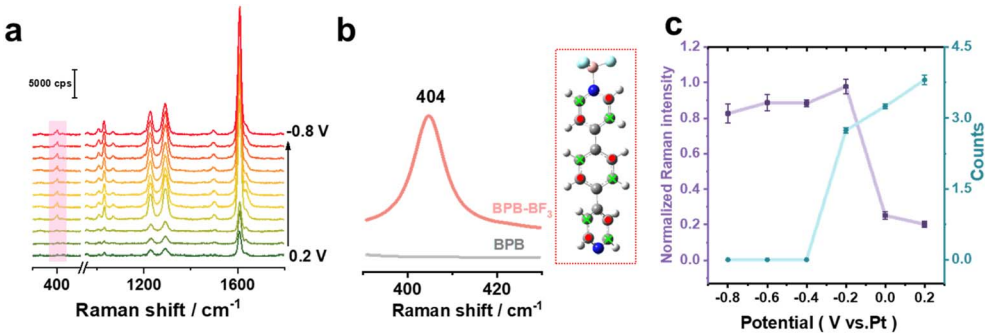

Fig. 3 (a) *In situ* Raman spectra obtained at Au(111) in 0.1 mM BPB + 30 mM $LiBF_4$ upon applied $E_{substrate}$ from 0.2 V to −0.8 V. (b) Theoretical simulated Raman spectra of τ_{cc} of the BPB–BF_3 Lewis adduct compared to that of isolated BPB. The illustration depicts a molecular structure, where red dots represent atoms vibrating outward, and green crosses indicate atoms vibrating inward. (c) Plot of the normalized intensities of the Raman band of τ_{cc} and conductance peak of the molecular junctions under different applied potentials.

observed throughout the entire electrochemical window, indicating that the molecule is stably adsorbed on the electrode surface *via* one of its pyridine groups. This further supports the idea that in the bulk solution, only one end of the molecular pyridine group forms a Lewis bond with BF_3, while the other pyridine group is uncoordinated and can bind to the gold electrode.

Interestingly, when the applied potential is reduced to −0.1 V and below, there is a sudden and significant increase in the intensities of the Raman bands associated with the molecules. At the same time, a new band appears at 403 cm^{-1}. According to the DFT simulations in Fig. 3b, compared with the isolated molecule, for the Lewis adduct with BF_3, a new Raman peak appears at 404 cm^{-1}, which is attributed to the CC out-of-plane twisting (τ_{cc}) vibration of the benzene ring and pyridine rings. In contrast, in the control experiment in $LiNO_3$ electrolyte solution (Fig. S15†), this Raman signal of τ_{cc} does not appear, and the other peak intensity of the molecule does not change significantly upon applied potential. This molecular evidence directly reveals that when the potential is reduced below the PZC, the molecules on the electrode surface form Lewis adducts with BF_3.

Fig. 3c compares the average normalized intensities of the Raman band of τ_{cc} from three independent experiments and conductance peak of molecular junctions under different applied potentials. The Raman intensity is normalized by the maximum peak area at 404 cm^{-1} in each dataset. Clearly, when the applied potential is lower than the PZC of −0.22 V, the intensity of the Raman peak of τ_{cc} increases abruptly, while the intensity of the conductance peak decreases sharply. This proves that the inward electric field generated at the negatively charged electrode surface promotes the formation of N–BF_3 Lewis adducts, preventing the formation of molecular junctions and causing the conductance peak to disappear. In addition, *in situ* Raman experiments in 50 mM $LiBF_4$ solution clearly show strong τ_{cc} in the potential range of 0.2 V to −0.8 V (Fig. S16†), because the increase in BF_3 concentration promotes the formation of N–BF_3 Lewis bonds. This further proves that the formation of N–BF_3 Lewis bonds prevents the Au-molecule contact from forming molecular junctions, consistent with the results of no conductance peak observed in the conductance measurement experiments.

Single-molecule contact switch

We next sought to further confirm our hypothesis of the electro-inductive effect controlled single-molecule contact switches. Conductance measurements of BPB were carried out upon cycling $E_{substrate}$ between 0 V and −0.6 V in 0.1 mM BPB + 30 mM $LiBF_4$ solution. The conductance histograms in Fig. S17† clearly show that a well-defined conductance peak at $10^{-4.0}$ G_0 repeatably appears at 0 V, but disappears at −0.6 V. Furthermore, 1,2-bis(4-pyridyl)ethylene (BPY-EE) and 4'-(pyridin-4-yl)-[1,1′-biphenyl]-4-carboxylic acid (PBBA) also show the same interesting switching phenomena upon changing the applied $E_{substrate}$ to generate different electro-inductive effects near the electrode surface. Detailed conductance histograms can be found in Fig. S18.† The different concentrations of $LiBF_4$ for BPY-EE and PBBA to achieve complete suppression of the conductance peaks might arise from their electronic structures, which might alter the strength of Lewis acid–base interactions between pyridinic nitrogen atoms and BF_3. The conductance peak disappears due to the formation of N–BF_3 Lewis bonds preventing the formation of molecular junctions, which means that the molecular circuit is disconnected (OFF state). Meanwhile, the positively charged surface generates the electron-withdrawing effects to break N–BF_3 Lewis bonds. Then, it promotes the formation of a molecular junction to allow electron tunnelling *via* the single-molecules, considered as a connection of the molecular circuit (ON state). Fig. 4a–c summarizes the results of repeatedly cycling the applied potentials followed by single-molecule conductance measurements. The conductance peaks at 0 V or −0.6 V appear and disappear repeatedly, clearly indicating that this single-molecule contact control is reversible. This demonstrates the good stability of single-molecule switches upon different electro-inductive effects.

To further test the molecule-contact switching in a fixed nanogap, we first constructed a single-molecule junction at 0 V in 0.1 mM BPB + 30 mM $LiBF_4$ solution. When a single-molecule

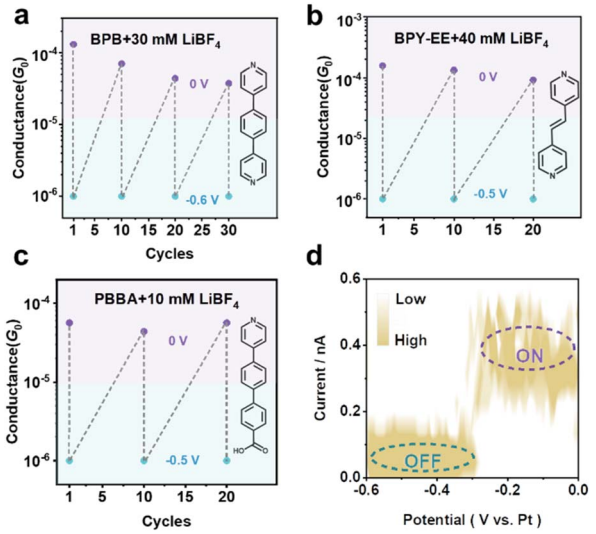

Fig. 4 Sequential cycles of conductance switching of (a) BPB, (b) BPY-EE and (c) PBBA between "ON" and "OFF" states. The purple dots are the conductance values obtained at 0 V after the different potential cycles, and the blue dots are positioned at 10^{-6} G_0 (the detection limit of the current signal amplifier) to indicate the disappearance of conductance peaks at −0.5 V or −0.6 V. The molecular structures are shown in the inset panels. (d) 2D *I*–*V* histogram of BPB obtained from dozens of data points when forming a single-molecule junction and sweeping the $E_{substrate}$ from 0 V to −0.6 V.

junction was formed, we hovered the STM tip above the substrate and performed *I*–*V* measurements. The experimental details can be found in the ESI.† The applied $E_{substrate}$ is swept from 0 V to −0.6 V, during which the electrode surface becomes negatively charged below the PZC and the initial electric field direction can be reversed to promote BF_3–pyridine interactions. Fig. S19† shows the typical *I*–*V* curve recorded upon the formation of molecular junctions. It is clear that the current jumps to the low current baseline during a negative potential sweep. This confirms that the electro-inductive effect induces the breaking of Au–N contacts in the molecular junction and forms N–BF_3 Lewis bonds. Fig. 4d shows the statistical results of the *I*–*V* curves collected at the formation of molecular junctions. The relative current difference is about 0.43 nA, which is comparable to single-molecule conductance in the break junction measurements. In addition, *I*–*t* tests according to previous reports[7] in 0.1 mM BPB + 30 mM $LiBF_4$ at an $E_{substrate}$ of 0 V confirm that the current jumps to the ON state due to junction formation, in contrast to only the base current observed at −0.6 V (Fig. S20†). These results further confirm that the electro-inductive effects at different applied potentials can modulate the Lewis chemistry between N and BF_3, leading to conductance ON/OFF switching.

Conclusions

We have successfully demonstrated that electro-inductive effects can be used to control the metal-molecule contact in a single-molecule junction, thus forming a type of connection-controlled molecular switch. Conductance measurements using the STM-BJ method clearly show that the single-molecule conductance peaks of heterocyclic molecules containing pyridyl groups become significantly weaker or even disappear when decreasing applied potentials to negatively charge an electrode surface in $LiBF_4$ solutions with different concentrations. Upon changing the electrolyte to $LiNO_3$ or using no pyridine groups, there is almost no change in the single-molecule conductance peak. Molecular evidence obtained by using UV-visible spectroscopy and *in situ* Raman spectroscopy reveals that the inward electric field along the negatively charged surface promotes the formation of the N–BF_3 Lewis bond between the BF_3 (liberated from $LiBF_4$ based on the equilibrium $BF_4^- \rightleftharpoons BF_3 + F^-$) and molecular pyridyl group. In contrast, the outward electric field along the electrode surface polarizes the adsorbed molecules to withdraw electron density from the terminal pyridine N, which weakens the N–BF_3 Lewis bond so it can dissociate upon applied positive potentials. With appropriate concentrations of $LiBF_4$ (*e.g.* 10–40 mM), the electro-inductive effect can lead to the single-molecule conductance peaks of BPY-EE and PBBA reversibly disappearing at low potentials and appearing at high potentials. This can be analogous to physically disconnecting and connecting molecule-metal contacts in single-molecule junctions to tune electron tunnelling. Furthermore, such metal-molecule contact switching is also demonstrated in a fixed nanogap between two electrodes in *I*–*V* measurements. This work sheds light on the electro-inductive effects on interfacial Lewis chemistry and opens a new avenue for the design of high-performance single-molecule switches.

Data availability

The data that support the findings of this study are available from the corresponding authors upon reasonable request.

Author contributions

Z. Y. L.: Conceived the theme of the paper and completed most of the experiments, discussions, data analysis, and wrote the manuscript; B. T. H.: Conducted surveys, completed part of the experiments, and participated in discussions and data interpretation; Y. J. T.: Theoretical aspect investigation, completed theoretical calculations, and interpreted the data; L. L. N.: Completed part of the experiments and participated in data analysis and discussions; W. Q.: Guided the theoretical calculations, participated in data analysis, and contributed to writing, reviewing, and editing the manuscript; Z. J. F.: Guided the paper, interpreted data, and reviewed the manuscript; S. Y.: Guided the paper, interpreted data, and reviewed the manuscript; W. Y. H.: Conceptualized and directed the project, conducted surveys, supervised, managed the project, secured funding, and wrote the manuscript; Z. X. S.: Conceptualized the study, conducted surveys, developed methodology, performed formal analysis, secured funding, and provided comments and edits.

Conflicts of interest

There are no conflicts to declare.

Acknowledgements

We acknowledge financial support from the National Natural Science Foundation of China (No. 22102150, 22172146, 22303085, and 21872126), and the Zhejiang Provincial Natural Science Foundation of China (No. LZ25B030003, LQ21B030010, LQ24B030014).

References

1 A. Aviram and M. A. Ratner, *Molecular Rectifiers, Chem. Phys. Lett.*, 1974, **29**, 277.
2 S. N. Lachmanová, V. Kolivoska, J. Sebera, J. Gasior, G. Mészáros, G. Dupeyre, P. P. Lainé and M. Hromadová, Environmental Control of Single-Molecule Junction Evolution and Conductance: A Case Study of Expanded Pyridinium Wiring, *Angew. Chem., Int. Ed.*, 2021, **60**, 4732–4739.
3 E. Leary, A. La Rosa, M. T. González, G. Rubio-Bollinger, N. Agraït and N. Martín, Incorporating Single Molecules into Electrical Circuits. The Role of the Chemical Anchoring Group, *Chem. Soc. Rev.*, 2015, **44**, 920–942.
4 B. Xu and N. J. Tao, Measurement of Single-Molecule Resistance by Repeated Formation of Molecular Junctions, *Science*, 2003, **301**, 1221–1223.
5 Q. Zhou, K. Song, G. Zhang, X. Song, J. Lin, Y. Zang, D. Zhang and D. Zhu, Tetrathiafulvalenes as anchors for building highly conductive and mechanically tunable molecular junctions, *Nat. Commun.*, 2022, **13**, 1803–1811.
6 L. Zhang, C. Yang, C. Lu, X. Li, Y. Guo, J. Zhang, J. Lin, Z. Li, C. Jia, J. Yang, K. N. Houk, F. Mo and X. Guo, Precise Electrical Gating of the Single-Molecule Mizoroki-Heck Reaction, *Nat. Commun.*, 2022, **13**, 4552.
7 L. Tong, Z. Yu, Y. J. Gao, X. C. Li, J. F. Zheng, Y. Shao, Y. H. Wang and X. S. Zhou, Local Cation-Tuned Reversible Single-Molecule Switch in Electric Double Layer, *Nat. Commun.*, 2023, **14**, 3397.
8 W. J. Hong, D. Z. Manrique, P. Moreno-García, M. Gulcur, A. Mishchenko, C. J. Lambert, M. R. Bryce and T. Wandlowski, Single Molecular Conductance of Tolanes: Experimental and Theoretical Study on the Junction Evolution Dependent on the Anchoring Group, *J. Am. Chem. Soc.*, 2012, **134**, 2292–2304.
9 F. Chen, X. Li, J. Hihath, Z. Huang and N. Tao, Effect of Anchoring Groups on Single-Molecule Conductance: Comparative Study of Thiol-, Amine-, and Carboxylic-Acid-Terminated Molecules, *J. Am. Chem. Soc.*, 2006, **128**, 15874–15881.
10 J. Prana, L. Kim, T. M. Czyszczon-Burton, G. Homann, S. F. Chen, Z. Miao, M. Camarasa-Gomez and M. S. Inkpen, Lewis-Acid Mediated Reactivity in Single-Molecule Junctions, *J. Am. Chem. Soc.*, 2024, **146**, 33265–33275.
11 U. Rashid, W. Bro-Jorgensen, K. B. Harilal, P. A. Sreelakshmi, R. R. Mondal, V. Chittari Pisharam, K. N. Parida, K. Geetharani, J. M. Hamill and V. Kaliginedi, Chemistry of the Au-Thiol Interface Through the Lens of Single-Molecule Flicker Noise Measurements, *J. Am. Chem. Soc.*, 2024, **146**, 9063–9073.
12 B.-F. Zeng, R. Deng, Y.-L. Zou, C.-A. Huo, J.-Y. Wang, W.-M. Yang, Q.-M. Liang, S.-J. Qiu, A. Feng, J. Shi, W. Hong, Z. Yang, Z.-Q. Tian and Y. Yang, Optical Trapping of a Single Molecule of Length Sub-1 nm in Solution, *CCS Chem.*, 2023, **5**, 830–840.
13 H. Chen, V. Brasiliense, J. Mo, L. Zhang, Y. Jiao, Z. Chen, L. O. Jones, G. He, Q.-H. Guo, X.-Y. Chen, B. Song, G. C. Schatz and J. F. Stoddart, Single-Molecule Charge Transport Through Positively Charged Electrostatic Anchors, *J. Am. Chem. Soc.*, 2021, **143**, 2886–2895.
14 L.-Q. Pei, J. R. Horsley, J.-W. Seng, X. Liu, Y. Q. Yeoh, M.-X. Yu, X.-H. Wu, A. D. Abell, J.-F. Zheng, X.-S. Zhou, J. Yu and S. Jin, Mechanically Induced Switching between Two Discrete Conductance States: A Potential Single-Molecule Variable Resistor, *ACS Appl. Mater. Interfaces*, 2021, **13**, 57646–57653.
15 X.-M. Li, Y.-H. Wang, J.-W. Seng, J.-F. Zheng, R. Cao, Y. Shao, J.-Z. Chen, J.-F. Li, X.-S. Zhou and B.-W. Mao, z-Piezo Pulse-Modulated STM Break Junction: Toward Single-Molecule Rectifiers with Dissimilar Metal Electrodes, *ACS Appl. Mater. Interfaces*, 2021, **13**, 8656–8663.
16 M. Kamenetska, S. Y. Quek, A. C. Whalley, M. L. Steigerwald, H. J. Choi, S. G. Louie, C. Nuckolls, M. S. Hybertsen, J. B. Neaton and L. Venkataraman, Conductance and Geometry of Pyridine-Linked Single-Molecule Junctions, *J. Am. Chem. Soc.*, 2010, **132**, 6817–6821.
17 K. Moth-Poulsen and T. Bjornholm, Molecular Electronics With Single Molecules in Solid-State Devices, *Nat. Nanotechnol.*, 2009, **4**, 551–556.
18 D. Stefani, K. J. Weiland, M. Skripnik, C. W. Hsu, M. L. Perrin, M. Mayor, F. Pauly and H. S. J. van der Zant, Large Conductance Variations in a Mechanosensitive Single-Molecule Junction, *Nano Lett.*, 2018, **18**, 5981–5988.
19 X. T. Wang, T. L. R. Bennett, A. Ismael, L. A. Wilkinson, J. Hamill, A. J. P. White, I. M. Grace, O. Kolosov, T. Albrecht, B. J. Robinson, N. J. Long, L. F. Cohen and C. J. Lambert, Scale-Up of Room-Temperature Constructive Quantum Interference from Single Molecules to Self-Assembled Molecular-Electronic Films, *J. Am. Chem. Soc.*, 2020, **142**, 8555–8560.
20 Q. Zou, J. Qiu, Y. Zang, H. Tian and L. Venkataraman, Modulating Single-Molecule Charge Transport Through External Stimulus, *eScience*, 2023, **3**, 100115.
21 W. Lee, L. Li, M. Camarasa-Gómez, D. Hernangómez-Pérez, X. Roy, F. Evers, M. S. Inkpen and L. Venkataraman, Photooxidation Driven Formation of Fe-Au Linked Ferrocene-Based Single-Molecule Junctions, *Nat. Commun.*, 2024, **15**, 1439.
22 J. S. Ward, A. Vezzoli, C. Wells, S. Bailey, S. P. Jarvis, C. J. Lambert, C. Robertson, R. J. Nichols and S. J. Higgins, A Systematic Study of Methyl Carbodithioate Esters as

Effective Gold Contact Groups for Single-Molecule Electronics, *Angew. Chem., Int. Ed.*, 2024, **63**, e202403577.
23 B. Huang, X. Liu, Y. Yuan, Z. W. Hong, J. F. Zheng, L. Q. Pei, Y. Shao, J. F. Li, X. S. Zhou, J. Z. Chen, S. Jin and B. W. Mao, Controlling and Observing Sharp-Valleyed Quantum Interference Effect in Single Molecular Junctions, *J. Am. Chem. Soc.*, 2018, **140**, 17685–17690.
24 J. M. Beebe, V. B. Engelkes, L. L. Miller and C. D. Frisbie, Contact Resistance in Metal−Molecule−Metal Junctions Based on Aliphatic SAMs: Effects of Surface Linker and Metal Work Function, *J. Am. Chem. Soc.*, 2002, **124**, 11268–11269.
25 J. G. Kushmerick, Metal-Molecule Contacts, *Mater. Today*, 2005, **8**, 26–30.
26 J. M. Seminario, C. E. De La Cruz and P. A. Derosa, A Theoretical Analysis of Metal−Molecule Contacts, *J. Am. Chem. Soc.*, 2001, **123**, 5616–5617.
27 Z. Liu, S. Y. Ding, Z. B. Chen, X. Wang, J. H. Tian, J. R. Anema, X. S. Zhou, D. Y. Wu, B. W. Mao, X. Xu, B. Ren and Z. Q. Tian, Revealing the Molecular Structure of Single-Molecule Junctions in Different Conductance States by fishing-Mode Tip-Enhanced Raman Spectroscopy, *Nat. Commun.*, 2011, **2**, 305.
28 L. Gerhard, K. Edelmann, J. Homberg, M. Valásek, S. G. Bahoosh, M. Lukas, F. Pauly, M. Mayor and W. Wulfhekel, An Electrically Actuated Molecular Toggle Switch, *Nat. Commun.*, 2017, **8**, 14672.
29 W. Haiss, C. Wang, I. Grace, A. S. Batsanov, D. J. Schiffrin, S. J. Higgins, M. R. Bryce, C. J. Lambert and R. J. Nichols, Precision Control of Single-Molecule Electrical Junctions, *Nat. Mater.*, 2006, **5**, 995–1002.
30 J. Li, P. Shen, S. Zhen, C. Tang, Y. Ye, D. Zhou, W. Hong, Z. Zhao and B. Z. Tang, Mechanical Single-Molecule Potentiometers With Large Switching Factors from Ortho-Pentaphenylene Foldamers, *Nat. Commun.*, 2021, **12**, 167.
31 H. Jeong, H. B. Li, L. Domulevicz and J. Hihath, An On-Chip Break Junction System for Combined Single-Molecule Conductance and Raman Spectroscopies, *Adv. Funct. Mater.*, 2020, **30**, 2000615.
32 X. N. Xu, C. Y. Gao, R. Emusani, C. C. Jia and D. Xiang, Toward Practical Single-Molecule/Atom Switches, *Adv. Sci.*, 2024, **11**, 2400877.
33 K. S. Westendorff, M. J. Hülsey, T. S. Wesley, Y. Román-Leshkov and Y. Surendranath, Electrically Driven Proton Transfer Promotes Brempty Setnsted Acid Catalysis by Orders of Magnitude, *Science*, 2024, **383**, 757–763.
34 S. D. Fried, S. Bagchi and S. G. Boxer, Extreme electric fields power catalysis in the active site of ketosteroid isomerase, *Science*, 2014, **346**, 1510–1514.
35 J. Heo, H. Ahn, J. Won, J. G. Son, H. K. Shon, T. G. Lee, S. W. Han and M. H. Baik, Electro-Inductive Effect: Electrodes as Functional Groups with Tunable Electronic Properties, *Science*, 2020, **370**, 214–219.
36 W. R. Lake, J. H. Meng, J. M. Dawlaty, T. Q. Lian and S. Hammes-Schiffer, Electro-inductive Effect Dominates Vibrational Frequency Shifts of Conjugated Probes on Gold Electrodes, *J. Am. Chem. Soc.*, 2023, **145**, 22548–22554.
37 S. Menachekanian, M. J. Voegtle, R. E. Warburton, S. Hammes-Schiffer and J. M. Dawlaty, Inductive Effect Alone Cannot Explain Lewis Adduct Formation and Dissociation at Electrode Interfaces, *J. Am. Chem. Soc.*, 2023, **145**, 5759–5768.
38 M. S. Hossain, A. I. B. Romo, S. T. Putnam, J. Dawlaty, V. Augustyn and J. Rodríguez-López, Electrode-Potential-Driven Dissociation of N-Heterocycle/BF3 Adducts: A Possible Manifestation of the Electro-Inductive Effect, *Angew. Chem., Int. Ed.*, 2023, **62**, e202304218.
39 Y. Zang, Q. Zou, T. Fu, F. Ng, B. Fowler, J. Yang, H. Li, M. L. Steigerwald, C. Nuckolls and L. Venkataraman, Directing Isomerization Reactions of Cumulenes with Electric Fields, *Nat. Commun.*, 2019, **10**, 4482.
40 X. S. Liu, S. Sangtarash, D. Reber, D. Zhang, H. Sadeghi, J. Shi, Z. Y. Xiao, W. J. Hong, C. J. Lambert and S. X. Liu, Gating of Quantum Interference in Molecular Junctions by Heteroatom Substitution, *Angew. Chem., Int. Ed.*, 2017, **56**, 173–176.
41 S. Afsari, P. Yasini, H. W. Peng, J. P. Perdew and E. Borguet, Anisotropic Conductivity at the Single-Molecule Scale, *Angew. Chem., Int. Ed.*, 2019, **58**, 14275–14280.
42 H. Wang, F. Hu, A. Adijiang, R. Emusani, J. Zhang, Q. Hu, X. Guo, T. Lee, L. Chen and D. Xiang, Gating the Rectifying Direction of Tunneling Current through Single-Molecule Junctions, *J. Am. Chem. Soc.*, 2024, **146**, 35347–35355.
43 J.-N. Jiang, Q. Wan, N. Sun, Y.-L. Zhang, B. Wang, J.-F. Zheng, Y. Shao, Y.-H. Wang and X.-S. Zhou, Label-Free Single-Molecule Electrical Sensor for Ultrasensitive and Selective Detection of Iodide Ions in Human Urine, *ACS Sensors*, 2024, **9**, 5578–5586.
44 Y. H. Wang, Y. F. Zhou, L. Tong, H. Huang, J. F. Zheng, W. Z. Xie, J. Z. Chen, Y. Shao and X. S. Zhou, Revealing Supramolecular Interactions and Electron Transport in Single Molecular Junctions of Cucurbit uril, *Adv. Electron. Mater.*, 2021, **7**, 2100399.
45 Y. H. Wang, X. C. Li, Z. Yu, J. F. Zheng and X. S. Zhou, Break-Junction Measurements at Electrochemical Interface: From Electron Transport to Molecular Adsorption and Reaction Process, *Curr. Opin. Electrochem.*, 2023, **39**, 101279.
46 C. Zhan, G. Wang, X. G. Zhang, Z. H. Li, J. Y. Wei, Y. Si, Y. Yang, W. J. Hong and Z. Q. Tian, Single-Molecule Measurement of Adsorption Free Energy at the Solid-Liquid Interface, *Angew. Chem., Int. Ed.*, 2019, **58**, 14534–14538.
47 C. P. Tao, C. C. Jiang, Y. H. Wang, J. F. Zheng, Y. Shao and X. S. Zhou, Single-Molecule Sensing of Interfacial Acid-Base Chemistry, *J. Phys. Chem. Lett.*, 2020, **11**, 10023–10028.
48 C.-P. Tao, C.-C. Jiang, Y.-H. Wang, J.-F. Zheng, Y. Shao and X.-S. Zhou, Single-Molecule Sensing of Interfacial Acid–Base Chemistry, *J. Phys. Chem. Lett.*, 2020, **11**, 10023–10028.
49 Y. X. Tang, Y. Zhou, D. H. Zhou, Y. R. Chen, Z. Y. Xiao, J. Shi, J. Y. Liu and W. J. Hong, Electric Field-Induced Assembly in Single-Stacking Terphenyl Junctions, *J. Am. Chem. Soc.*, 2020, **142**, 19101–19109.
50 Z. Yan, X. X. Li, Y. S. Li, C. C. Jia, N. Xin, P. H. Li, L. A. Meng, M. Zhang, L. Chen, J. L. Yang, R. M. Wang and X. F. Guo,

Single-Molecule Field Effect and Conductance Switching Driven by Electric Field and Proton Transfer, *Sci. Adv.*, 2022, **8**, 7.

51 Z. Yu, Y. X. Xu, J. Q. Su, P. M. Radjenovic, Y. H. Wang, J. F. Zheng, B. T. Teng, Y. Shao, X. S. Zhou and J. F. Li, Probing Interfacial Electronic Effects on Single-Molecule Adsorption Geometry and Electron Transport at Atomically Flat Surfaces, *Angew. Chem., Int. Ed.*, 2021, **60**, 15452–15458.

52 Y. H. Wang, J. B. Le, W. Q. Li, J. Wei, P. M. Radjenovic, H. Zhang, X. S. Zhou, J. Cheng, Z. Q. Tian and J. F. Li, In situ Spectroscopic Insight into the Origin of the Enhanced Performance of Bimetallic Nanocatalysts towards the Oxygen Reduction Reaction (ORR), *Angew. Chem., Int. Ed.*, 2019, **58**, 16062–16066.

53 J. F. Li, Y. F. Huang, Y. Ding, Z. L. Yang, S. B. Li, X. S. Zhou, F. R. Fan, W. Zhang, Z. Y. Zhou, D. Y. Wu, B. Ren, Z. L. Wang and Z. Q. Tian, Shell-Isolated Nanoparticle-Enhanced Raman Spectroscopy, *Nature*, 2010, **464**, 392–395.

54 Z. Yu, J.-Q. Li, Y.-H. Wang, J.-Q. Su, J.-Y. Fu, J.-W. Zou, J.-F. Zheng, Y. Shao and X.-S. Zhou, Visualizing an Electrochemically Induced Radical Cation of Bipyridine at Au(111)/Ionic Liquid Interfaces toward a Single-Molecule Switch, *Anal. Chem.*, 2022, **94**, 1823–1830.